Chinese Physics Letters

LETTER

Pairing Symmetry and Superconductivity in $La_3Ni_2O_7$ Thin Films

Cite as: Wenyuan Qiu *et al*. 2026 *Chin. Phys. Lett.* **43** 080710

DOI CSTR

Recommended Articles

Pairing Mechanism and Superconductivity in 1313 Phase $La_3Ni_2O_7$

Cui-Qun Chen, Ming Zhang, Fan Yang, and Dao-Xin Yao
Chin. Phys. Lett. **43**, 070711 (2026)

High-Temperature Superconductivity in $La_3Ni_2O_7$

Kun Jiang, Ziqiang Wang, and Fu-Chun Zhang
Chin. Phys. Lett. **41**, (2024)

Superexchanges and Charge Transfer in $La_3Ni_2O_7$ Thin Films

Yuxun Zhong, Wéi Wú, and Dao-Xin Yao
Chin. Phys. Lett. **43**, 030713 (2026)

The Effect of Carrier Doping and Thickness on the Electronic Structures of $La_3Ni_2O_7$ Thin Films

Haoliang Shi, Zihao Huo, Guanlin Li, Hao Ma, Tian Cui, Daoxin Yao, and Defang Duan
Chin. Phys. Lett. **42**, 080708 (2025)

Normal and Superconducting Properties of $La_3Ni_2O_7$

Meng Wang, Hai-Hu Wen, Tao Wu, Dao-Xin Yao, and Tao Xiang
Chin. Phys. Lett. **41**, (2024)

Detecting Pairing Symmetry of Bilayer Nickelates Using Electronic Raman Scattering

Jun Zhan, Matías Bejas, Andreas P. Schnyder, Andrés Greco, Xianxin Wu, and Jiangping Hu
Chin. Phys. Lett. **43**, 020706 (2026)

A series journal of Chinese Physical Society distributed by IOP Publishing

Chinese Physics Letters

Chin. Phys. Lett. **43** 080710 (2026)

LETTER

DOI: 10.1088/0256-307X/43/8/080710
CSTR: 32039.14.0256-307X.43.8.080710

Pairing Symmetry and Superconductivity in $La_3Ni_2O_7$ Thin Films

Wenyuan Qiu(邱文渊)[1,†], Zhihui Luo(罗志辉)[1,†], Xunwu Hu(胡训武)[2], and Dao-Xin Yao(姚道新)[1,*]

[1]Institute of Neutron Science and Technology, State Key Laboratory of Optoelectronic Materials and Technologies, School of Physics, Sun Yat-Sen University, Guangzhou 510275, China
[2]Department of Physics, College of Physics and Optoelectronic Engineering, Jinan University, Guangzhou 510632, China

[†]These authors contributed equally to this work
[*]Corresponding author. Email: yaodaox@mail.sysu.edu.cn

The recent discovery of superconductivity with a transition temperature T_c over 40 K in $La_3Ni_2O_7$ and $(La,Pr)_3Ni_2O_7$ thin films at ambient pressure marks an important step in the field of nickelate superconductors. Here, we perform a renormalized mean-field theory study of the superconductivity in $La_3Ni_2O_7$ thin films, using a bilayer two-orbital t–J model. Our result reveals an $s_\pm$-wave pairing symmetry driven by the strong interlayer superexchange coupling of d_{z^2} orbital, resembling the pressurized bulk case. Also, we roughly reproduce the experimentally observed nodeless shape of the superconducting gap at the β pocket and the superconducting T_c. In addition, by analysing the orbital-resolved pairing configurations and their projections onto Fermi surface, we find that the nodeless feature of β pocket is related to the interlayer pairing within both d_{z^2} and $d_{x^2-y^2}$ orbitals. Moreover, we identify a formation of the inplane inter-orbital d-wave pairing between d_{z^2} and $d_{x^2-y^2}$ orbitals, which can even enhance the dominated interlayer $s_\pm$-wave. Our study particularly highlights the diverse relations of different pairing channels in $La_3Ni_2O_7$ that holds a complex Fermi surface.

Introduction

The discovery of superconductivity with a transition temperature T_c near 80 K in the Ruddlesden-Popper (RP) bilayer nickelate $La_3Ni_2O_7$ (LNO) [1] has gained widespread interests in the field of high-T_c superconductivity, and it was soon followed by another observation of superconductivity in trilayer nickelate $La_4Ni_3O_{10}$ with T_c = 20–30 K [2,3], both under high pressure. The discovery of RP nickelate-based superconductors has marked a breakthrough in the field of high-T_c superconductivity, and therefore raised considerable subsequent investigations both theoretically [4–38] and experimentally [3,39–45]. However, the need for high pressure has largely confined some critical experimental techniques for a direct probe of the superconducting phase, such as angle resolved photoemission spectroscopy (ARPES) and scanning tunneling microscopy (STM), which prevents a decisive confirmation of the superconducting pairing among various theoretical proposals [16,34]. On the other hand, achieving ambient-pressure superconductivity is a crucial step for practical considerations, and in this respect, there are some suggestions on the possible route, such as using chemical substitute [46–49] or applying strain [50–53].

Very recently, superconductivity with T_c over 40 K in LNO [54] and $(La,Pr)_3Ni_2O_7$ [55] thin films at ambient pressure have been reported. The X-ray absorption spectroscopy (XAS) analysis and scanning transmission electron microscopy (STEM) reveal that, the Ni ions in LNO thin films maintain a mixed valence state and the apical Ni-O-Ni bond angle approaches 180° [54], which closely resembles the high-pressure bulk phase of LNO. The ARPES measurement [56] in thin films also confirms the dominant Ni-$d_{x^2-y^2}$ and d_{z^2} orbital spectral weights around the Fermi energy, which is consistent with DFT calculations [52,53,57–59]. Moreover, a direct ARPES measurement of the superconducting electronic structure on the Fermi surface (FS) was performed recently [60], which reveals a notable gap opening on the β FS sheet and without showing any node along the Brillouin zone (BZ) diagonal direction. This observation is accompanied by another STM measurement on superconducting state [61], which shows a two-gap structure on the FS and a fitting to such gaps demonstrates a preferable anisotropic s-wave pairing. The two results are generally prone to the idea of the predominant $s_\pm$-wave pairing symmetry in the system as predicted by several theoretical studies [7,16,18,35,58].

In this paper, using a bilayer $t-J$ model that captures the key ingredient of LNO thin films, we perform a renormalized mean-field theory (RMFT) [7] calculation of the superconductivity. Our result reveals the $s_\pm$-wave pairing and reproduces the experimentally observed nodeless shape of the superconducting gap at β pocket in Ref. [60]. To gain insight, we also analyse the orbital-resolved pairing bonds and their projections onto Fermi surface. Our study highlights the diverse relations of different pairing channels in LNO that holds a complex Fermi surface.

Model and Method

The bilayer two-orbital $t-J$ model is defined as

$$\mathcal{H} = \mathcal{H}_t + \mathcal{H}_J, \tag{1}$$

$$\mathcal{H}_t = \sum_{ij}\sum_{\mu\nu}\sum_{\sigma} t_{ij}^{\mu\nu} c_{i\mu\sigma}^{\dagger} c_{j\nu\sigma} - \mu \sum_{i\mu\sigma} n_{i\mu\sigma}, \tag{2}$$

$$\mathcal{H}_J = J_\perp \sum_i \boldsymbol{S}_{iz_1}\cdot\boldsymbol{S}_{iz_2} + J_\parallel \sum_{\langle ij\rangle}^{\mu=x_1,x_2} \boldsymbol{S}_{i\mu}\cdot\boldsymbol{S}_{j\mu} + J_{xz} \sum_{\langle ij\rangle}^{\mu\nu=x_1z_1,x_2z_2} \boldsymbol{S}_{i\mu}\cdot\boldsymbol{S}_{j\nu} - J_H \sum_i^{\mu\nu=x_1z_1,x_2z_2} \boldsymbol{S}_{i\mu}\cdot\boldsymbol{S}_{i\nu}. \tag{3}$$

In this model, the basis is $\Psi = (d_{z_1}, d_{x_1}, d_{z_2}, d_{x_2})^{\mathrm{T}}$ that contains d_{z^2} and $d_{x^2-y^2}$ orbitals for the first and second layers, as shown in Fig. 1(b). $\mathcal{H}_t$ is the tight-binding Hamiltonian adopted from DFT simulation for the double-stacked LNO thin films [57]. Here, ij, $\mu\nu$, σ denote the lattice, orbital, and spin indices, respectively. The band structure is shown in Fig. 1(a), in which a small electron doping level with chemical potential $\mu = 0.05$ is used in our calculation to better agree

Received 6 May 2026; accepted 18 July 2026; published 19 August 2026
© 2026 Chinese Physical Society and IOP Publishing Ltd. All rights, including for text and data mining, AI training, and similar technologies, are reserved.

Check for updates

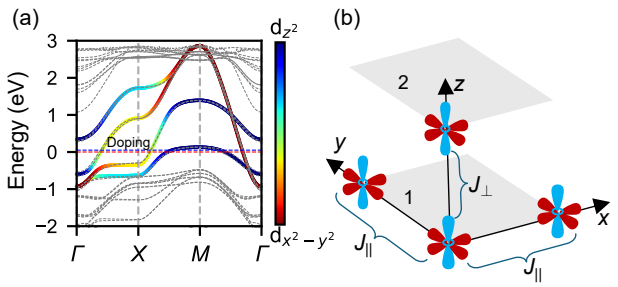

Fig. 1. (a) Band structure of the 4-orbital tight-binding model adopted from the DFT simulation of the double-stacked $La_3Ni_2O_7$ thin film [57]. The red dashed line denotes the undoped case from DFT while the blue one denotes the slightly electron doped case as is used in our study. (b) Schematic of $d_{x^2-y^2}$ (red) and d_{z^2} (blue) orbitals of the model. Two major superexchange couplings $J_\perp$, $J_\parallel$ are drawn. See also the main text.

with the experiments, which gives the electron filling n_z=0.8, n_x=0.58. We found that by slightly adjusting the filling, the resulting γ pocket around the M point becomes noticeably closer to the ARPES observations [62]. The observation of Sr diffusion from substrates might explain the differences of electron filling between experiments and theories [63]. For the Heisenberg term $\mathcal{H}_J$, $J_\perp$ is the interlayer superexchange coupling of d_{z^2} orbitals, and $J_\parallel, J_{xz}$ are the inplane nearest neighbor superexchange coupling of $d_{x^2-y^2}$ orbital, and superexchange coupling between $d_{x^2-y^2}$ and d_{z^2}, respectively. Also, the Hund's coupling J_H is included for generality. To quantitatively estimate $J_\perp, J_\parallel, J_{xz}$, we perform the exact diagonalization (ED) calculation and obtain $J_\perp$ = 0.135 eV, $J_\parallel$ = 0.084 eV, J_{xz} = 0.03 eV. Taking $J_\perp$ as an example, ED is performed for a 5-site chain containing two d_{z^2} and three p_z orbitals along the z axis, with p−d hoppings obtained from DFT [57]. Under the atomic subspace that corresponds to half-filling of d_{z^2} orbital ($N = 8$, $S_z = 0$), $J_\perp$ is determined as the energy difference of the lowest singlet and triplet states [8]. Similar method is applied in Refs. [64,65]. Besides, a realistic J_H = 1 eV is also used in this study.

The above $t-J$ model is solved under the RMFT. The RMFT [66] follows a conventional mean-field decomposition of spin exchange, which yields the order parameters $\chi_{ij}^{\mu\nu} = \langle c_{i\mu\uparrow}^\dagger c_{jv\uparrow}\rangle$ and $\Delta_{ij}^{\mu\nu} = \langle c_{i\mu\uparrow}^\dagger c_{jv\downarrow}^\dagger\rangle$ under the spin symmetry. Besides, $\mathcal{H}_t$ and $\mathcal{H}_J$ are respectively coupled by the Gutzwiller renormalization factors g_t and g_J to recover the strong renormalization from correlation [67]. The obtained quadratic Hamiltonian is then calculated self-consistently, during which the electron densities are fixed to certain level. The eventual pairing symmetry can be determined from the phase structure of various pairing bonds $\Delta_{ij}^{\mu\nu}$. For the inplane pairing, this is done by allowing Δ along x and y directions to evolve independently, so a final $s_\pm$,d wave or s+id wave is possible depending on the superexchanges. We refer reader to Ref. [7] for details of the method.

Pairing Symmetry and Superconducting Gap

Figure 2(a) presents the superconducting gap matrix $[g_t\Delta]_{\mu\nu}$ projected onto FS, which demonstrates that β,γ pockets are nodeless and of opposite sign, while α pocket shows a sign flip. To better illustrate the gap features, figures 2(b)–2(d) show the absolute value $g_t|\Delta|$ as a function of angle θ for α, β, and γ pockets, respectively. For α pocket in Fig. 2(b), the gap demonstrates a node between $\theta = 45° - 90°$. For β pocket in Fig. 2(c), the gap shows a parabolic shape centering at $\theta = 45°$, which gets slightly decrease when approaching the corner. Note that the gap shape as well as its magnitude around the BZ diagonal direction from our result are generally coordinated with the ARPES result [60], which suggests that our RMFT captures the key ingredient in the LNO thin films. For γ pocket in Fig. 2(d), we find the gap magnitude is about 5 times larger than that in Fig. 2(b), with its minimum appearing at the BZ diagonal direction. Apparently, such large gap opening at γ pocket should be attributed to the strong interlayer superexchange coupling $J_\perp$, which is also consistent with previous calculations for bulk LNO [7,16,18,25]. Overall, the pairing structure in Fig. 2 should be described as the $s_\pm$-wave, which can also be seen from our result that besides the formation of the large interlayer pairing bond for d_{z^2} orbital ($\Delta_\perp^z$), the inplane pairing bonds have the same magnitude when along x,y directions for both $d_{x^2-y^2}$ and d_{z^2} orbitals ($\Delta_\parallel^x, \Delta_\parallel^z$). Note that, in our $t-J$ model only the pairing bonds $\Delta_\perp^z, \Delta_\parallel^x, \Delta_\parallel^{xz}$ are associated with the applied $J_\perp, J_\parallel, J_{xz}$, respectively, while other terms like the interlayer pairing of $d_{x^2-y^2}$ orbital ($\Delta_\perp^x$) do not have the corresponding J and should not appear in the calculation. However, they can still gain finite values as $\Delta_{ij}^{\mu\nu} = \langle n\mathbf{k}|c_{i\mu\uparrow}^\dagger c_{jv\downarrow}^\dagger|n\mathbf{k}\rangle$, which reflects the pairing tendency towards a global coherent state at the mean-field level. In the following we will dive into the role of different pairing bonds to see how they interplay and collectively give rise to the result in Fig. 2.

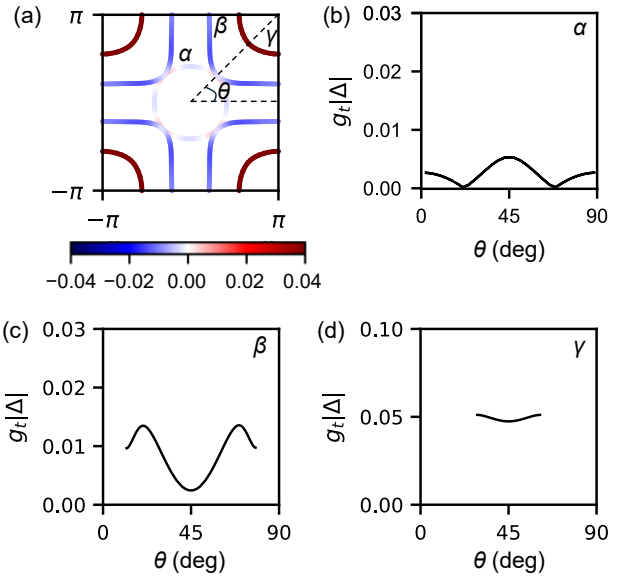

Fig. 2. (a) Superconducting gap $g_t\Delta$ projected onto FS for $La_3Ni_2O_7$ thin films. (b)–(d) $g_t|\Delta|$ as a function of angle θ for α, β, and γ pockets, respectively. θ is indicated in (a).

Orbital-Resolved Superconducting Gap

Figure 3 presents the orbital-resolved superconducting gap for (a) $\Delta_\perp^z$, (b) $\Delta_\parallel^z$, (c) $\Delta_\perp^x$, and (d) $\Delta_\parallel^x$, respectively. For $\Delta_\perp^z$ in Fig. 3(a), the gap is positive for the bonding branch of α,γ pockets, and is negative for the anti-bonding branch of β pocket. For $\Delta_\parallel^z$ in Fig. 3(b), the gap structure clearly demonstrates the sign-flip $s_\pm$-wave with the node appearing at the extended BZ boundary (diamond shape). Also, another node at the BZ diagonal direction in both Figs. 3(a) and 3(b) is identified due to the vanishing of hybridization. For $\Delta_\perp^x, \Delta_\parallel^x$ in Figs. 3(c) and 3(d), similar behavior is observed as compared to Figs. 3(a) and 3(b), but with a much smaller magnitude. It is worth noting that the phases in Figs. 3(a)–3(d) all can be understood in terms of maximizing the total gap magnitude. Because the large $J_\perp$ will guarantee $\Delta_\perp^z$ to be the leading pairing, other pairings in Figs. 3(c) and 3(d) will have to fit into it. First, figure 3(c) will choose the same sign that matches Fig. 3(a) ($\mathrm{sgn}\Delta_\perp^z = \mathrm{sgn}\Delta_\perp^x$). This does not conflict with their spatial configuration as the two sides are both connected by J_H. This result clearly explains the experimentally observed nodeless shape of β pocket as a joint effort of interlayer pairing for both $d_{x^2-y^2}$ and d_{z^2} orbitals. Second, due to the inplane $\cos k_x + \cos k_y$ form factor in Figs. 3(b) and 3(d), cancelation of the gap in certain region of FS is unavoidable, which inherently reflects the "pairing frustration". In this case $\Delta_\parallel^z$ will choose to maximize the gap for γ pocket at the price of minimizing the gap for α pocket, while $\Delta_\parallel^x$ will no doubt choose to maximize the gap for α pocket, with slight cancelation at β pocket. In

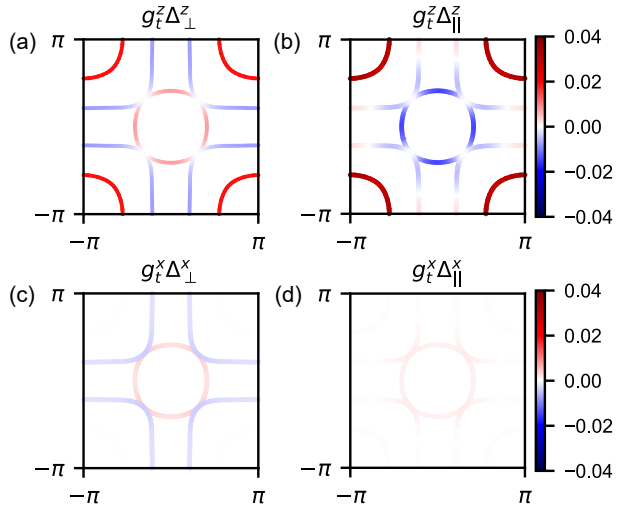

Fig. 3. Orbital-resolved superconducting energy gap on FS for (a) $\Delta_\perp^z$, (b) $\Delta_\parallel^z$, (c) $\Delta_\perp^x$, and (d) $\Delta_\parallel^x$. $g_t^{z/x}$ is the renormalization factor for $d_{z^2}/d_{x^2-y^2}$ orbital. $\Delta_{\perp/\parallel}^{z/x}$ denotes the interlayer/inplane pairing bond for $d_{z^2}/d_{x^2-y^2}$ orbital.

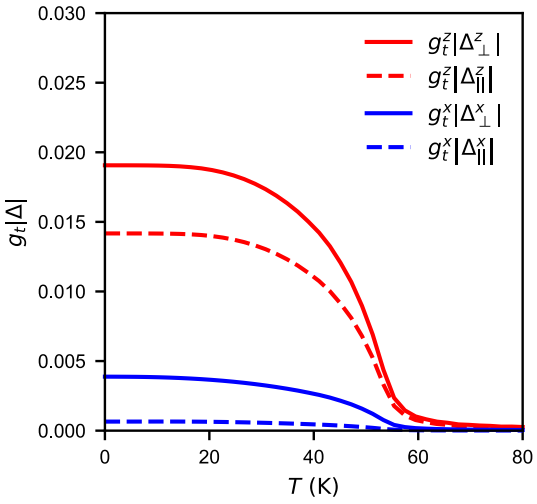

Fig. 4. Superconducting gap as a function of temperature for different pairing bonds. $g_t^{z/x}$ is the renormalization factor for $d_{z^2}/d_{x^2-y^2}$ orbital, and $\Delta_{\perp/\parallel}^{z/x}$ is the interlayer/inplane pairing bond for $d_{z^2}/d_{x^2-y^2}$ orbital.

this sense, "pairing frustration" is more likely to occur in system with multi-orbital feature and complex Fermi surface where there can not find a single pairing symmetry to perfectly fit in with. More insights into it and the "gap maximization" via free energy functional is provided in the Supplemental Material (SM). In LNO, the obtained gap relation is $\mathrm{sgn}\Delta_\perp^z = \mathrm{sgn}\Delta_\perp^x = \mathrm{sgn}\Delta_\parallel^x = -\mathrm{sgn}\Delta_\parallel^z$. General agreements can be found in Refs. [18,31]. Finally, concerning the inplane inter-orbital pairing $\Delta_\parallel^{xz}$, surprisedly, we find it actually forms a d-wave and can even enhance the dominated $\Delta_\perp^z$. This is a unique feature for LNO tetrahedral lattice where the two distinct pairings can coexist within A_{1g} channel, see the SM and Ref. [68] for details.

Temperature Dependence of Superconducting Gap

In Fig. 4, we show the superconducting gap as a function of temperature T, which reveals two dominated pairing bonds from d_{z^2} orbitals (red), in line with Fig. 3. As increasing T, these gaps decrease in a mean-field manner and simultaneously drop to zero at $T_c \approx 60$ K. Such value is comparable to the experimental reported T_c = 40–60 K in the thin films [50,54,55]. Given that our previous RMFT study also obtains an experimental comparable $T_c \approx 80$ K for the pressurized bulk LNO [7], it is reasonable to believe that the decrease of T_c in the thin films should originate from the decrease of $J_\perp$. This speculation draws us to the difference in the electronic structure, especially in the mainly concerned interlayer hopping $t_\perp^z$ for d_{z^2} orbital. Notably, we find that the $J_\perp$ = 0.135 eV in this study is ~ 25% smaller than that of $J_\perp$ = 0.18 eV for the pressurized bulk [8] as estimated from ED, which is coordinated with a simple estimation using $J_\perp \propto (t_\perp^z)^2$ [4,57]. Recently, a strain-tuning experiment in LNO thin films reports an increase of T_c from 10 K in the tensile-strained $SrTiO_3$ substrate to 60 K in the compressively strained $LaAlO_3$ substrate under 20 GPa of pressure [50]. Recently, other groups also reported T_c over 60 K in bilayer nickelate thin films through applying hydrostatic pressure [69,70]. This indicates a positive dependence of T_c on the lattice ratio c/a and, at first glance, violates the above understanding. However, we tend to believe $J_\perp$ can only determine the upper bound of T_c, while other factors like hybridization, density wave, and interlayer Josephson coupling can also have intricate impact, as also pointed out in Ref. [50,71−76].

Discussion and Conclusion

Our RMFT study of the superconductivity in LNO thin films has predicted an $s_\pm$-wave pairing symmetry. The result largely resembles that of the pressurized bulk LNO [7,16,18,25] giving the similarity in the electronic structure. Mathematically, our application of Gutzwiller projection [18,66] on a multi-orbital $t-J$ model imposes a constraint on the renormalization condition to make the renormalization factor depends only on the orbital densities [7,77], so the RMFT formation can be solved self-consistently like the standard Bardeen-Cooper-Schrieffer (BCS) theory. Therefore, it is expected that the obtained $s_\pm$-wave mainly reflects pairing preference for the LNO FS topology in the presence of $J_\perp$ [78]. Nevertheless, we find that the $s_\pm$-wave is quite robust under various approaches from weak to strong couplings, which convinces us that the fluctuation of correlated atomic states might not significantly alter such scenario. In this scenario, the γ pocket plays a central role. Experimentally, there are two relevant ARPES measurements in which the γ pocket shows visible profile for that performed in the normal state [56] but invisible for that in the superconducting state [51]. From our result, this contradiction might be due to the opening of a large gap that exceeds the detected energy range, as shown Fig. 2(d). More experimental evidences are expected on this issue. Regarding the role of J_H, no significant impact is observed from our approach at the singlet pairing channel. We see that J_H mainly contributes to an effective interlayer correlation of $d_{x^2-y^2}$ orbitals.

However, in real materials, many factors will influence the pairing symmetry in $La_3Ni_2O_7$ thin films, such as substrate-induced strain, oxygen vacancies and interfacial effects. These factors are expected to influence the pairing symmetry through modifications to the electronic structure, such as the Fermi surface, hopping amplitudes, and superexchange couplings. Substrate-induced compressive strain suppresses the γ pocket and increases the c/a ratio [79], which reduces both the interlayer d_{z^2} hopping and corresponding superexchange couplings [57]. Meanwhile, apical oxygen vacancies disrupt the Ni–O–Ni bonds along the c-axis, weakening the interlayer d_{z^2} superexchange coupling. Conversely, Sr diffusion from the substrate effectively introduce hole doping, which promotes the appearance of the γ pocket [62,63]. Within the RMFT framework, the absence of the γ pocket drives the d_{z^2} orbital toward half-filling, suppressing the interlayer $s_\pm$ gap, and the reduction in $J_\perp$ further diminishes the interlayer $s_\pm$ pairing tendency.

To summarize, we perform a RMFT study of the superconductivity in the LNO thin films using a bilayer $t-J$ model. Our result reveals an $s_\pm$-wave pairing symmetry driven by the interlayer superexchange coupling, resembling the bulk LNO case. Our result also roughly reproduces the experimentally reported nodeless shape of the superconducting gap at β pocket [60] as well as the superconducting T_c. In addition, we systematically analyse the relation between orbital-resolved pairing bonds and the gap structure on FS. The result shows that the nodeless gap of β pocket is related to the interlayer

pairing within both d_{z^2} and $d_{x^2-y^2}$ orbitals. We also find the formation of inplane inter-orbital d-wave pairing between $d_{x^2-y^2}$ and d_{z^2} orbitals that can enhance the dominated interlayer $s_\pm$-wave. The coexistence is robust symmetrically in $La_3Ni_2O_7$ lattice.

Acknowledgements

We thank the useful discussion with Wéi Wú, Guan-Hao Feng. This project was supported by the National Natural Science Foundation of China (Grant Nos.12494591 and 92565303), the National Key R&D Program of China (Grant No. 2022YFA1402802), the Guangdong Provincial Key Laboratory of Magnetoelectric Physics and Devices (Grant No. 2022B1212010008), the Research Center for Magnetoelectric Physics of Guangdong Province (Grant No. 2024B0303390001), and the Guangdong Provincial Quantum Science Strategic Initiative (Grant No. GDZX2401010).

References

[1] Sun H, Huo M, Hu X *et al*. 2023 *Nature* **621** 493
[2] Zhu Y, Peng D, Zhang E *et al*. 2024 *Nature* **631** 531
[3] Li Q, Zhang Y J, Xiang Z N *et al*. 2024 *Chin. Phys. Lett.* **41** 017401
[4] Luo Z, Hu X, Wang M *et al*. 2023 *Phys. Rev. Lett.* **131** 126001
[5] Zhang Y, Lin L F, Moreo A *et al*. 2023 *Phys. Rev. B* **108** L180510
[6] Lechermann F, Gondolf J, Bötzel S *et al*. 2023 *Phys. Rev. B* **108** L201121
[7] Luo Z, Lv B, Wang M *et al*. 2024 *npj Quantum Mater.* **9** 1
[8] Wú W, Luo Z, Yao D X *et al*. 2024 *Sci. China Phys. Mech. Astron.* **67** 117402
[9] Wang M, Wen H H, Wu T *et al*. 2024 *Chin. Phys. Lett.* **41** 077402
[10] Shilenko D and Leonov I 2023 *Phys. Rev. B* **108** 125105
[11] Yang Y F, Zhang G M, and Zhang F C 2023 *Phys. Rev. B* **108** L201108
[12] Huang J, Wang Z, and Zhou T 2023 *Phys. Rev. B* **108** 174501
[13] Christiansson V, Petocchi F, and Werner P 2023 *Phys. Rev. Lett.* **131** 206501
[14] Shen Y, Qin M, and Zhang G M 2023 *Chin. Phys. Lett.* **40** 127401
[15] Oh H and Zhang Y H 2023 *Phys. Rev. B* **108** 174511
[16] Liu Y B, Mei J W, Ye F *et al*. 2023 *Phys. Rev. Lett.* **131** 236002
[17] Liao Z, Chen L, Duan G *et al*. 2023 *Phys. Rev. B* **108** 214522
[18] Yang Q G, Wang D, and Wang Q H 2023 *Phys. Rev. B* **108** L140505
[19] Chen C Q, Luo Z, Wang M *et al*. 2024 *Phys. Rev. B* **110** 014503
[20] Xu S, Chen C Q, Huo M *et al*. 2025 *Phys. Rev. B* **111** 075140
[21] Yang J J, Yao D X, and Wu H Q 2024 *Phys. Rev. B* **110** 235155
[22] Ouyang Z, Gao M, and Lu Z Y 2024 *npj Quantum Mater.* **9** 1
[23] Sakakibara H, Ochi M, Nagata H *et al*. 2024 *Phys. Rev. B* **109** 144511
[24] Heier G, Park K, and Savrasov S 2024 *Phys. Rev. B* **109** 104508
[25] Zhang Y, Lin L F, Moreo A *et al*. 2024 *Nat. Commun.* **15** 2470
[26] Zhang Y, Lin L F, Moreo A *et al*. 2024 *Phys. Rev. B* **109** 045151
[27] Tian Y H, Chen Y, Wang J M *et al*. 2024 *Phys. Rev. B* **109** 165154
[28] Ryee S, Witt N, and Wehling T 2024 *Phys. Rev. Lett.* **133** 096002
[29] Zhang J X, Zhang H K, You Y Z *et al*. 2024 *Phys. Rev. Lett.* **133** 126501
[30] Ni X S, Ji Y, He L *et al*. 2025 *npj Quantum Mater.* **10** 1
[31] Lu C, Pan Z, Yang F *et al*. 2024 *Phys. Rev. Lett.* **132** 146002
[32] Qu X Z, Qu D W, Chen J *et al*. 2024 *Phys. Rev. Lett.* **132** 036502
[33] Yang H, Oh H, and Zhang Y H 2024 *Phys. Rev. B* **110** 104517
[34] Fan Z, Zhang J F, Zhan B *et al*. 2024 *Phys. Rev. B* **110** 024514
[35] Sakakibara H, Kitamine N, Ochi M *et al*. 2024 *Phys. Rev. Lett.* **132** 106002
[36] Cao Y and Yang Y F 2024 *Phys. Rev. B* **109** L081105
[37] Jiang R, Hou J, Fan Z *et al*. 2024 *Phys. Rev. Lett.* **132** 126503
[38] Chen X, Jiang P, Li J *et al*. 2025 *Phys. Rev. B* **111** 014515
[39] Yang J, Sun H, Hu X *et al*. 2024 *Nat. Commun.* **15** 4373
[40] Zhang Y, Su D, Huang Y *et al*. 2024 *Nat. Phys.* **20** 1269
[41] Hou J, Yang P T, Liu Z Y *et al*. 2023 *Chin. Phys. Lett.* **40** 117302
[42] Fan S, Luo Z, Huo M *et al*. 2024 *Phys. Rev. B* **110** 134520
[43] Wang G, Wang N, Shen X *et al*. 2024 *Phys. Rev. X* **14** 011040
[44] Liu Z, Huo M, Li J *et al*. 2024 *Nat. Commun.* **15** 7570
[45] Li J, Peng D, Ma P *et al*. 2025 *Natl. Sci. Rev.* **12** nwaf220
[46] Pan Z, Lu C, Yang F *et al*. 2024 *Chin. Phys. Lett.* **41** 087401
[47] Zhang Y, Lin L F, Moreo A *et al*. 2023 *Phys. Rev. B* **108** 165141
[48] Li F, Xing Z, Peng D *et al*. 2025 *Nature* **649** 871
[49] Qiu Z, Chen J, Semenok D *et al*. 2025 arXiv: 2510.12359 [cond-mat.supr-con]
[50] Osada M, Terakura C, Kikkawa A *et al*. 2025 *Commun. Phys.* **8** 251
[51] Wang B, Zhong Y, Abadi S *et al*. 2025 arXiv: 2504.16372 [cond-mat.supr-con]
[52] Bhatt L, Jiang A, Ko E *et al*. 2025 arXiv: 2501.08204 [cond-mat.supr-con]
[53] Liu Y, Ko E, Tarn Y *et al*. 2025 arXiv: 2501.08022 [cond-mat.supr-con]
[54] Ko E, Yu Y, Liu Y *et al*. 2025 *Nature* **638** 935
[55] Zhou G, Lv W, Wang H *et al*. 2025 *Nature* **640** 641
[56] Li P, Zhou G, Lv W *et al*. 2025 arXiv: 2501.09255 [cond-mat.supr-con]
[57] Hu X, Qiu W, Chen C Q *et al*. 2025 *Commun. Phys.* **8** 506
[58] Yue C, Miao J J, Huang H *et al*. 2025 *Natl. Sci. Rev.* **12** nwaf253
[59] Shi H, Huo Z, Li G *et al*. 2025 arXiv: 2502.04255 [cond-mat.supr-con]
[60] Shen J, Miao Y, Ou Z *et al*. 2026 *Science* **392** 1396
[61] Fan S, Ou M, Scholten M *et al*. 2025 arXiv: 2506.01788 [cond-mat.supr-con]
[62] Li P, Zhou G, Lv W *et al*. 2025 *Natl. Sci. Rev.* **12** nwaf205
[63] Li G, Chen C Q, Shi H *et al*. 2025 arXiv: 2512.17625 [cond-mat.supr-con]
[64] Zhou Y, Zhao D, Zeng B *et al*. 2025 arXiv: 2505.09476 [cond-mat.supr-con]
[65] Jiang G, Qin C, Foyevtsova K *et al*. 2025 *Sci. China Phys. Mech. Astron.* **68** 297411
[66] Zhang F, Gros C, Rice T *et al*. 1988 *Supercond. Sci. Technol.* **1** 36
[67] Gutzwiller M 1965 *Phys. Rev.* **137** A1726
[68] Feng G H, Quan J, and Hou Y 2025 arXiv: 2506.01764 [cond-mat.supr-con]
[69] Li Q, Sun J, Bötzel S *et al*. 2026 *Nat. Commun.* **17** 3276
[70] Zhao J, Zhou G, Cai S *et al*. 2026 arXiv: 2603.29531 [cond-mat.supr-con]
[71] Qin Q and Yang Y F 2023 *Phys. Rev. B* **108** L140504
[72] Chen K, Liu X, Jiao J *et al*. 2024 *Phys. Rev. Lett.* **132** 256503
[73] Meng Y, Yang Y, Sun H *et al*. 2024 *Nat. Commun.* **15** 10408
[74] Zhang M, Chen C Q, Yao D X *et al*. 2025 arXiv: 2505.15906 [cond-mat.supr-con]
[75] Khasanov R, Hicken T, Gawryluk D *et al*. 2025 *Nat. Phys.* **21** 430
[76] Zheng Y Y and Wú W 2025 *Phys. Rev. B* **111** 035108
[77] Edegger B, Muthukumar V, and Gros C 2007 *Adv. Phys.* **56** 927
[78] Hu J and Ding H 2012 *Sci. Rep.* **2** 381
[79] Zhao Y F and Botana A 2025 *Phys. Rev. B* **111** 115154